Materials Horizons

ROYAL SOCIETY OF CHEMISTRY

COMMUNICATION

View Article Online
View Journal | View Issue

Cite this: *Mater. Horiz.*, 2024, **11**, 4961

Received 17th April 2024,
Accepted 27th June 2024

DOI: 10.1039/d4mh00454j

rsc.li/materials-horizons

Fault-tolerant computing with single-qudit encoding in a molecular spin†

Matteo Mezzadri, ‡[ab] Alessandro Chiesa, ‡[abc] Luca Lepori [ab] and Stefano Carretta *[abc]

We show that molecular spins represent ideal materials to realize a fault-tolerant quantum computer, in which all quantum operations include protection against leading (dephasing) errors. This is achieved by pursuing a qudit approach, in which logical error-corrected qubits are encoded in a single multi-level molecule (a qudit) and not in a large collection of two-level systems, as in standard codes. By preventing such an explosion of resources, this emerging way of thinking about quantum error correction makes its actual implementation using molecular spins much closer. We show how to perform all quantum computing operations (logical gates, corrections and measurements) without propagating errors. We achieve a quasi-exponential error correction with only linear qudit size growth, *i.e.* a higher efficiency than the standard approach based on stabilizer codes and concatenation.

New concepts

We introduce the first procedure for the fault-tolerant implementation of a universal set of quantum operations on error-corrected qubits encoded in molecular spins. Such a fault-tolerant implementation (which tolerates errors during computation without propagating them) is mandatory to realize a useful quantum computer. Our novel concept exploits specific features of molecular spins and, in particular, of molecular nanomagnets, *i.e.* the presence of many levels which can be coherently manipulated, and their unparalleled tunability at the synthetic levels. The former is exploited to follow a qudit approach and encode an error-corrected qubit into a single molecule, thus preventing the explosion of resources typical of existing multi-qubit codes. The latter allows us to design a fault-tolerant methodology to actually implement gates and error correction on a realistic platform, thus making a crucial step forward. The remarkable performance obtained in realistic simulations on a wide class of molecular spins demonstrates the great potential of these materials as viable a path for fault-tolerant quantum computation. Moreover, our work highlights which simple molecules could represent a new generation of logical qubits. Noticeably, we do not find stringent requirements for spin coherence, thus greatly simplifying the synthesis of suitable molecules.

1 Introduction

A "useful" quantum computer should be universal, accurate and scalable.[1] Meeting these conditions on noisy hardware requires a fault-tolerant quantum error correction (QEC) approach, which allows for universal quantum computation with an arbitrary error reduction, while remaining experimentally achievable.

The standard way to tackle this problem relies on encoding the elementary unit of computation (a logical qubit, LQ) into a collection of distinct physical qubits.[2–6] Different codes were developed along these lines, progressively increasing the maximum tolerated error for each elementary operation (the so-called threshold).[7–16] However, all of them show an explosion in the number of physical qubits and gates to achieve error suppression required for reliable computation,[12,17,18] which represents an important roadblock to an actual implementation.

We follow an orthogonal approach, in which the elementary protected unit of information is encoded in a single d-level qudit (thus dramatically reducing the resource overhead), and we show that molecular spins provide ideal qudits to achieve a fault-tolerant (FT) implementation. Indeed, molecular spin qudits (MSQs) meet two key requirements for FT quantum computation: (i) they show a clear hierarchy in the errors affecting the system, with dephasing largely dominant.[19–21] (ii) They can accommodate many low-energy eigenstates whose properties can be tuned to a large extent at the synthetic level.[21–23] Note that a FT implementation, in which errors do not propagate during quantum operations, is of primary importance for any QEC scheme.[24] Otherwise, correction procedures would amplify the errors handled by the code, making the procedure practically useless. Although the idea of embedded codes[19,23,25–28] has recently inspired other proposals based on

[a] *Università di Parma, Dipartimento di Scienze Matematiche, Fisiche e Informatiche, I-43124 Parma, Italy. E-mail: stefano.carretta@unipr.it*
[b] *Gruppo Collegato di Parma, INFN-Sezione Milano-Bicocca, I-43124 Parma, Italy*
[c] *UdR Parma, INSTM, I-43124 Parma, Italy*

† Electronic supplementary information (ESI) available. See DOI: https://doi.org/10.1039/d4mh00454j

‡ These authors contributed equally to this work.

MSQs[19–21,29,30] or photons,[27,28,31–37] a comprehensive fault-tolerant (FT) implementation accommodating realistic noise models, noisy ancillae, encodings, measurements, and especially noise during a universal set of gates, is still missing.[24,28]

Here, we propose the first fault-tolerant implementation of an embedded stabilizer code for MSQs, in which all quantum computing (QC) steps (*i.e.* a universal set of logical operations, stabilization and correction) are transparent to the errors handled by the code, *i.e.* errors do not propagate during any of these operations.

We first introduce an illustrative class of simple MSQs which can be used as elementary units of quantum hardware and their coupling with the environment. Thanks to a clear hierarchy in the error operators, a code which protects them from the most relevant ones can be derived. Then, we propose a scheme which makes all QC procedures (one- and two-qubit logical gates, stabilization and recovery) error transparent (ET) by appropriate pulse sequences. Based on numerical simulations, we investigated the performance of the code (the so-called threshold analysis), showing that the corrected qubit beats the uncorrected one even for short coherence times. This significantly lowers the requirements for the molecular hardware. Moreover, we find an almost exponential error correction with only a linear growth in the number of qudit levels.

We also highlight the possibility of applying the code to different classes of molecular spins meeting the requirements we have identified of a well-defined hierarchy in the errors and a high connectivity between the eigenstates.

2 Results and discussion

2.1 Molecular spin quantum hardware

As a prototypical example of a MSQ suitable for the proposed FTQC scheme, we consider a giant-spin S molecule with non-axial zero-field splitting anisotropy. The total spin $S \geq 3/2$ can arise either from a single ion or from the interaction between different local spins in the so-called single-molecule magnets. This class of systems was widely studied by chemists and physicists for information storage, with the target of increasing the anisotropy barrier and hence the axial character of the molecule.[38–42] Here, we relax the requirement of strong axial anisotropy and consider a system (labeled as **1**) described by the following Hamiltonian:

$$H_S = DS_z^2 + E(S_x^2 - S_y^2) + \mu_B B g S_z, \quad (1)$$

where D and E parameterize the axial and rhombic zero-field splitting anisotropy of the system, while the last term indicates the Zeeman interaction with an external field along z. Note that in the case of multi-spin single-molecule magnets S represents the total spin of the ground multiplet, which can be rather

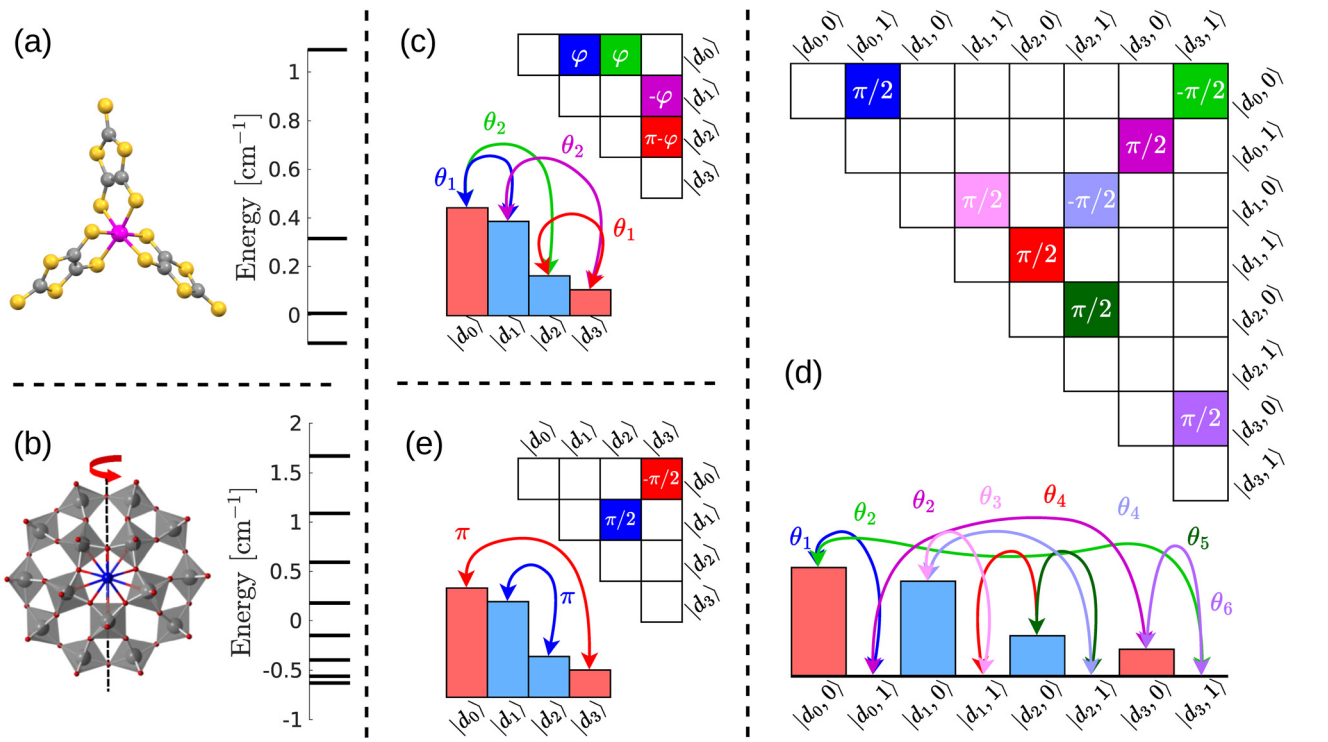

Fig. 1 Examples of single-ion magnets suitable for the implementation of our protocol: spin S = 3/2 $[Cr(C_3S_5)_3]^{3-}$ (a)[46] and S = 7/2 GdW_{30} (b).[47] The energy level diagram obtained from diagonalization of Hamiltonian (1) at 0.35 T. Scheme of single-qubit gates (c), stabilization (d), and recovery (e) for a S = 3/2 LQ (d = 4 levels), using the code words reported in Table 1. In each panel, the histogram represents the populations of eigenstates in blue (orange) for ℓ = 0(1). The upper triangular matrix on the right is the driving Hamiltonian in the rotating frame, with filled boxes indicating the set of θ_i resonant pulses between pairs of eigenstates (arrows in the histograms) simultaneously sent to the system. Different colors of the arrows and boxes indicate different pulse frequencies, while the phases are indicated at the top. For stabilization (d), the eigenstates of a two-level ancilla (0,1) are also reported. (b) Reprinted (figure) with permission from ref. 47, Copyright (2017) by the American Physical Society.

large.[43,44] In the following, we consider a typical experimental magnetic field, $B = 0.35$ T, and we set $D = -0.81$ cm^{-1} $\approx$ 24 GHz and $E = -0.24$ cm^{-1} $\approx$ 7 GHz for $S = 3/2$. Then, we investigate the FT implementation of QEC codes for different values of S ranging from 3/2 to 11/2, corresponding to qudits of dimension $d = 4,\ldots,12$. By varying S, we consider a reduction in D, E and B by a common factor $S(2S-1)$§ to maintain the frequency of the resonant pulses used for manipulation in an experimentally feasible range. Note that the performance of the scheme is not influenced by such a re-scaling of all the parameters, because the system eigenstates and the corresponding dephasing processes are not changed. The sizable rhombic anisotropy (not negligible with respect to axial anisotropy and Zeeman splitting) in (1) ensures that all required transitions between the d levels used for the encoding can be individually and efficiently addressed by resonant microwave pulses. We stress that these parameters can already be found in existing compounds, such as the molecules reported in Fig. 1(a) and (b). These are the spin 3/2 Cr-based qudit $[Cr(C_3S_5)_3]^{3-}$,[46] showing $E/D \approx 1/3$ and $T_2 \sim 2$ μs and the $S = 7/2$ GdW_{30} complex,[47] again with high rhombicity $E/D \sim 0.23$. This feature is specifically exploited in the FT implementation of our protocol. It is important to stress that this choice of parameters is not critical. In fact, a smaller E/D would reduce the value of some of the required magnetic dipole matrix elements, but without hindering the feasibility of our scheme. Indeed, this reduction can be compensated for by increasing the amplitude of the driving field or by the presence of higher-rank zero-field splitting operators (typically present for $S > 3/2$). In addition, the signs of D and E are irrelevant to our scheme.

Furthermore, the required connectivity can be obtained even with very different MSQs, such as anti-ferromagnetically coupled spin clusters with competing exchange interactions, as proposed in ref. 23 and 48. The performance of an illustrative example of this class of molecules (labeled as **2** and described in the ESI†) will also be considered for comparison in the following. Noteworthily, the proposed methodology does not introduce stringent requirements for coherence times (see below), thus greatly simplifying the synthetic efforts.

Errors corrupting quantum information initially encoded in the pure state $\rho_0 = |\psi_0\rangle\langle\psi_0|$ can be, in general, represented by Kraus operators E_k, *i.e.* the density matrix after possible errors is $\rho = \sum_k E_k \rho_0 E_k^\dagger$. Protection against a set of errors $\{E_k\}$ can be achieved by identifying code words $|0_L\rangle$ and $|1_L\rangle$, which satisfy Knill–Laflamme conditions (KLc):[49]

$$\langle 0_L|E_k^\dagger E_j|0_L\rangle = \langle 1_L|E_k^\dagger E_j|1_L\rangle \quad (2a)$$

$$\langle 0_L|E_k^\dagger E_j|1_L\rangle = 0. \quad (2b)$$

By using d-dimensional qudits (*i.e.* d levels of the spin Hamiltonian for the encoding), at most $d/2$ different errors can be corrected. We then consider the vector set $\{E_k|0_L\rangle, E_k|1_L\rangle\}_{k=0}^{d/2-1}$, and the orthonormal basis set $\mathscr{A}$ obtained from its Gram–Schmidt orthogonalization. We denote the set $\mathscr{A}$ as $\{\ell,k\}$ with $\ell = 0, 1$ labeling the logical states and $k = 0,\ldots,d/2-1$ as the correctable errors.

In MSQs (as in trapped ions,[50,51] atoms[52] and several other spin architectures[53,54]), pure dephasing (with decay time T_2) is the leading error at low temperature, while spin–lattice relaxation (T_1) is orders of magnitude slower.[46,55,56] Therefore in the following we will focus on it.

Pure dephasing in MSQs arises from the coupling between the system spins and the surrounding nuclear spins.[20,57] In the secular and Born–Markov approximations, one can derive a Lindblad equation for the evolution of the density matrix (see ESI†),[23,48] resulting in a decay of only the off-diagonal terms of ρ [$\rho_{ij}(t) = \rho_{ij}(0)e^{-\gamma_{ij}t}$] with rates $\gamma_{ij} = \sum C^{zz}_{kk'}[\langle d_i|s^z_k|d_i\rangle\langle d_i|s^z_{k'}|d_i\rangle + \langle d_j|s^z_k|d_j\rangle\langle d_j|s^z_{k'}|d_j\rangle - 2\langle d_i|s^z_k|d_i\rangle\langle d_j|s^z_{k'}|d_j\rangle]$. These are essentially related to the structure of the eigenstates $|d_i\rangle$, $|d_j\rangle$, apart from the coefficients $C^{zz}_{kk'}$ that depend on the dipolar interactions between the system and bath spins and, hence, on the relative positions between them (see the ESI†)¶. Although these are system-specific, the general conclusions that follow are not.[23,48] Note that the matrix elements of the local spin operators in system **1** are proportional to the giant spin operators within the ground multiplet, *i.e.* $\langle d_i|s^z_k|d_i\rangle \propto \langle d_i|S_z|d_i\rangle$.

From the solution of the Lindblad equation, we obtain the system density matrix at time t subject to pure dephasing, $\rho_{ij}(t) = \rho_{ij}(0)e^{-\gamma_{ij}t}$. This expression for ρ can be re-written as a Kraus decomposition at a fixed time t, $\rho(t) = \sum_k E_k \rho(0) E_k^\dagger$, with diagonal operators E_k. The latter can then be determined by state tomography.[58] Since they display a clear hierarchical structure, we focus on the $d/2$ most relevant ones and solve KLc (2). For instance, the E_k operators for a spin $S = 3/2$ giant spin **1** ($d = 4$) are reported in Table 1 (left), in order of decreasing norm. E_0 and E_1 (in bold) are clearly leading and we can write a set of equations to fulfill KLc for them, thus determining the code words reported in Table 1 (right) and the whole orthonormal set $\{|\ell,k\rangle\}$ in the eigenbasis (different columns). The magnitudes of the components of the code

Table 1 Left: elements of the diagonal error operators E_k, $k = 0, 1, 2, 3$, for $S = 3/2$, based on the eigenvectors $|d_k\rangle$ of Hamiltonian H_S in eqn (1), obtained by process tomography of the system subject to pure dephasing. Right: corresponding orthonormal set of error words $\mathscr{A}$ satisfying the Knill–Laflamme conditions [eqn (2)] for the error diagonal operators E_k reported on the left side

Kraus operators					Codewords and error words				
E_k	$\|d_0\rangle\langle d_0\|$	$\|d_1\rangle\langle d_1\|$	$\|d_2\rangle\langle d_2\|$	$\|d_3\rangle\langle d_3\|$	$\|\ell,k\rangle$	$\|d_0\rangle$	$\|d_1\rangle$	$\|d_2\rangle$	$\|d_3\rangle$
E_0	$\mathbf{9.9988 \times 10^{-01}}$	$\mathbf{9.9918 \times 10^{-01}}$	$\mathbf{9.9996 \times 10^{-01}}$	$\mathbf{9.9888 \times 10^{-01}}$	$\|0,0\rangle$	0	8.5335×10^{-01}	5.2135×10^{-01}	0
E_1	$\mathbf{1.5707 \times 10^{-02}}$	$\mathbf{4.0417 \times 10^{-02}}$	$\mathbf{-8.8440 \times 10^{-03}}$	$\mathbf{-4.7298 \times 10^{-02}}$	$\|0,1\rangle$	0	5.2135×10^{-01}	-8.5335×10^{-01}	0
E_2	-4.7091×10^{-04}	6.6400×10^{-04}	-7.4171×10^{-04}	5.4969×10^{-04}	$\|1,0\rangle$	9.2188×10^{-01}	0	0	3.8748×10^{-01}
E_3	8.2900×10^{-06}	-2.9673×10^{-06}	-6.8142×10^{-06}	1.4916×10^{-06}	$\|1,1\rangle$	-3.8748×10^{-01}	0	0	9.2188×10^{-01}

words in the eigenbasis are shown by the bars in Fig. 1, where different colors indicate components of different logical states $\ell = 0, 1$. A simple choice is to define $\ell = 0$ and $\ell = 1$ logical subspaces disjoint in the eigenbasis. For instance, in the example of Fig. 1, $\ell = 0$ is encoded onto eigenstates $|d_0\rangle$ and $|d_3\rangle$, while $\ell = 1$ is encoded onto $|d_1\rangle$ and $|d_2\rangle$. We have tested with different parameters in the spin Hamiltonian and spatial distributions of nuclear spins that the hierarchical structure of the errors is rather general. The other E_k operators and the corresponding code words are reported in the ESI,† for different S or, in general, for different numbers of qudit eigenstates ($d = 4$ to 12) used to define the LQ. Note that by changing d we are actually changing the code and, hence, a threshold analysis for each case is needed (see below).

2.2 Fault-tolerant implementation

Based on this molecular spin hardware, we now formally discuss the FT implementation of the logical gates. Given a gate G on a single qubit, the corresponding logical gate G_L that extends G to the protected LQ is given by $G_L \doteq G \otimes I_{d/2}$. This means applying the gate G to each subspace $|\ell,k\rangle$ independent of k and highlights the basic idea to achieve FTQC, *i.e.* to perform logical operations independent of the error.[37] Two-qubit controlled logical gates CG can be realized in a similar way, by implementing CG independent of the error k on both the control and target LQs (see the ESI†).

Let us start with a logical planar rotation $R_L^P(\theta,\phi) = \exp[-i(\cos\phi\ Y_L - \sin\phi\ X_L)\theta/2]$, as shown in Fig. 1(c). Its ET realization requires resonant pulses between each eigenstate in the logical $\ell = 0$ subspace [blue bars in Fig. 1(c)] and each one in the logical $\ell = 1$ subspace (orange bars). Hence, the system Hamiltonian must ensure the possibility of directly driving magnetic dipole transitions between each pair of eigenstates in the two subspaces. Remarkably, this is granted by both **1** and **2** for the proper choice of subspaces and of driving pulses. Different pulses of length θ_j are indicated by double arrows in the histogram, and their phase φ_j is reported in the connectivity matrix $\tilde{H}$ nearby. As detailed in the ESI,† one can show (with a generalized rotating frame formalism[59]) that the set of simultaneous pulses $\{\theta_j,\varphi_j\}$ implements the unitary $\exp[-i\tilde{H}]$, which corresponds to $R_L^P(\theta,\phi)$. Here, we assume all the energy gaps to be spectroscopically distinguishable. Remarkably, since $\theta, \varphi \in \mathbb{R}$, the resulting set of gates $R_L^P(\theta,\phi)$ is a universal set for one-body logical operation. Along the same lines, one can also implement a two-body ET $C-\varphi$ logical gate in a single step (see below).

We now turn to the steps of error detection and correction. Error detection is achieved by measuring

$$\Sigma = \sum_{k,\ell} \lambda_k |\ell,k\rangle\langle\ell,k| \tag{3}$$

where $\lambda_k \neq \lambda_{k'}$ for $k \neq k'$. This corresponds to the stabilization of information used in stabilizer codes on qubits, with the important simplification that we have only one multi-valued stabilizer Σ that gives directly the error syndrome instead of multiple two-valued stabilizers,[60,61] *i.e.* the code is nondegenerate. This reduces the impact of measurement errors (see below). Even more importantly, this enables the direct identification of errors starting from the syndrome, without needing a syndrome decoder, which is usually an important bottleneck for large qubit stabilizer codes.[62,63]

Stabilization is achieved by exploiting a $d/2$-level ancilla linked to the d-level LQ and implementing a k-controlled operation CU between the LQ (control, initially in a generic state $|\bar{\psi}\rangle$) and ancilla (target, initialized in its ground state 0). The CU gate acts as follows: $|\ell,k\rangle|0\rangle \mapsto |\ell,k\rangle|k\rangle$, $|\ell,k\rangle|k\rangle \mapsto -|\ell,k\rangle|0\rangle$ and the identity otherwise.‖ Therefore, CU maps each error k to a specific eigenstate of the ancilla. Hence, a final measurement of the ancilla in its eigenbasis identifies the error syndrome k and stabilizes the information in the subspace $|\ell,k\rangle$. Note that CU is ET since it does not affect the state of the LQ but only the state of the ancilla.

The implementation of a CU on the MSQ is shown in Fig. 1(d). In this case, the eigenstates of both the LQ and of a $d/2$ level ancilla are shown in the product basis $|d_j,k\rangle$, with the ancilla initialized in its ground state $|0\rangle$. In this 4-level example, stabilization requires exciting the ancilla iff LQ is $k = 1$. This translates into the set of simultaneous pulses shown in Fig. 1(d) between each qudit eigenstate $|d_i\rangle$ with the ancilla in $|0\rangle$ and each qudit eigenstate $|d_j\rangle$ with the ancilla in $|1\rangle$. Following the argument above, one can derive the connectivity matrix with pulse lengths and phases by taking the logarithm of the CU gate (see the ESI†). For logical gates, the required connectivity for stabilization is ensured by both the proposed model systems (see the ESI† for details). The ancilla could be an additional smaller giant spin unit with $S' = S/2 - 1/4$, S being the total spin of LQ. Remarkably, the ancilla does not need to be encoded. Indeed, it is excited to the eigenstate $|k\rangle$ with the same probability p_k and an error E_k. Hence, it suffers an error $E_{k'}$ with the conditional probability $p_k p_{k'}$, which results to be of a higher order than the error in the qudit.

The recovery (correction) step R_k^L simply consists of mapping back the stabilized states $|\ell,k\rangle$ into $|\ell,0\rangle$ by a unitary transformation depending on k. Since R_k^L can be written as $I_2 \otimes R_k$, no evolution between subspaces with different values of ℓ is performed. The implementation of R_k^L from $k = 1$ to $k = 0$ (for the specific case $d = 4$) is illustrated in Fig. 1(e), and is obtained by a pair of pulses within the two disjoint $\ell = 0, 1$ subspaces.**

To conclude, we describe how to measure and initialize a LQ. In particular, readout of the LQ state corresponds to the measurement of Z_L, which again translates into distinguishing the value of ℓ independent of the error k. Having chosen the $\ell = 0$ and $\ell = 1$ logical subspaces disjoint in the eigenbasis, the readout simply corresponds to summing the probabilities of finding the LQ into the eigenstates belonging to each of the two subspaces (either $|d_0\rangle$ and $|d_3\rangle$ or $|d_1\rangle$ and $|d_2\rangle$ in the above example). Reading out the state of a molecular spin qudit can be done by coupling it with a superconducting resonator[64] and borrowing strategies used for superconducting qubits, as shown in the blueprint in ref. 65. In this setup, control lines are used to implement single-qudit operations *via* classical driving pulses at different frequencies, while the qudit readout is achieved by exploiting its strong coupling with the quantized photon field in the resonator.

At last, LQ encoding can be achieved analogously to standard qubit stabilizer codes.[7,9] Starting from the qudit into its ground eigenstate, we drive it to the proper superposition of eigenstates defining $|0_L\rangle \equiv |0,0\rangle$. Errors that occur during this step bring the system to a mixture $\sum_{\ell\ell' kk'} \rho_{\ell,k}^{\ell',k'} |\ell,k\rangle\langle\ell',k'|$. Hence, we first perform a logical measurement of the qudit discarding it if we get an $\ell = 1$ outcome, and we finally proceed with a stabilization step, discarding it for any $k \neq 0$.

Summarizing, we have presented MSQs characterized by two key requirements to achieve FTQC, *i.e.* (i) a clear hierarchical structure in the error operators and (ii) the capability to implement in a single step any QC operation U of the embedded QEC protocol. This is achieved by driving the system *via* proper resonant oscillating fields ($\tilde{H} = i \log U$) directly inducing transitions between the qudit eigenstates. In practice, this implies suitable connectivity between the qudit eigenstates that can be obtained in MSQs, owing to the high degree of chemical tunability of the Hamiltonian in this class of systems.[21,22,66–71]

2.3 Threshold analysis

We now show the effectiveness of our scheme for the correction of pure dephasing errors (with characteristic time T_2) in MSQs. This is done by numerically integrating the Lindblad equation for the system density matrix, subject to both pure dephasing and the sequence of pulses required to implement the desired operations (see the ESI†). These include a universal set of logical gates, stabilization (CU), and recovery. We also consider possible measurement errors (see below). In contrast to standard threshold analysis,[12] we do not assume discrete errors occurring with a given probability but a continuous dephasing realistically describing the system and acting during all of the procedures, with an elementary error rate of $1/T_2$.††

We start by considering generic $R_L^P(\theta,\phi)$ rotations, followed by stabilization and correction. We report the final logical error $\bar{\mathscr{E}}_e$ as a function of the elementary error rate $1/T_2$ for molecule **1** in Fig. 2(a). Here, $\mathscr{E}_e = 1 - \mathscr{F}_e^2$, where $\mathscr{F}_e$ is the entanglement fidelity of the procedure,‡‡[72] and we average on a universal set of (θ,ϕ) values. The logical error is obtained by full-state tomography of the logical state and corresponds to the failure probability of the QEC protocol, *i.e.* errors that cannot be corrected by the code.

We immediately note that the slope of the curves in Fig. 2(a) on the log–log scale for the LQ (number of levels ≥ 4) is larger than that for the uncorrected case (blue line). This means that $\bar{\mathscr{E}}_e$ is propagated through the executed circuit to a higher order than the elementary error, thus remarking the fault tolerance of all procedures involved. Notably, for reasonable gate duration (90 ns for the LQ, see§§[73–75] and ESI†), the LQ with $d = 4$ ($S = 3/2$) beats the uncorrected two-level system for $T_2 \gtrsim 1$ μs, a perfectly achievable value in MSQs.[56,57,73] This corresponds to an error probability for the elementary transition between a pair of qudit levels of $p \gtrsim \tau/2T_2 \approx 4.5\%$. By increasing d (*i.e.* considering a qudit with a larger S), the codes outperform spin 1/2 independent of T_2. This behavior is an important strength of our method, which ensures FTQC without any stringent requirement on molecular T_2 (or on elementary error probability). Indeed, the errors are reduced and propagated to higher orders, as evidenced by the increase of the slope of the curves in Fig. 2(a). It is also worth noting that, although molecule **2** is very different from **1**, the results for the final logical error after the application of the same procedure are perfectly analogous [see the inset of Fig. 2(a)].

Remarkably, we find for both **1** and **2** an almost exponential suppression of the error with a linear increase of d, as reported in Fig. 2(b), independent of T_2. This makes the proposed protocol much more efficient than the standard qubit concatenation techniques, where an exponential error suppression is obtained with an exponential growth of the Hilbert space.[58] To quantify this gain, we note that the final error suppression is strikingly larger; here, we achieve a logical error of 10^{-12} by employing 12×6 levels (LQ + ancilla) and $T_2 = 10$ μs, which should be compared to more than 5000 qubits needed by Floquet codes with the same elementary error $p \approx \tau/2T_2 = 0.45\%$.[18] This remarkable performance, which only requires proper connectivity between the molecular eigenstates, is found here by focusing on the dominant family of errors of molecular systems. Moreover, the depth of our circuit (*i.e.* the number of operations implemented in sequence) does not increase with d. Indeed, all operations are implemented in parallel, again in contrast to standard codes. Remarkably, here, a single measurement is sufficient for syndrome extraction, and the corresponding error[76] can be suppressed by repeated measures, as shown by simulations in the ESI.†

Leakage errors could arise due to the finite duration of the pulses can be largely reduced by pulse-shaping techniques[77] and/or by using longer pulses. Indeed, increasing the length of the pulses simply shifts the curves in Fig. 2 to the left without changing the slope. This will slightly increase the threshold value of T_2 without compromising the fault tolerance. It is worth noting that most of the line broadening typically observed in electron paramagnetic resonance experiments on MSQs arises from the distribution of Hamiltonian parameters or orientations in molecular ensembles. Conversely, QEC requires projective measurements at each correction cycle; hence, it can only be implemented at the single-molecule level, exploiting the setup mentioned in Section 2.1 and designed in ref. 65. In this case, inhomogeneous broadening is absent and the residual intrinsic linewidth originating from T_2 will be of the order of $1/T_2 \sim 0.1$ MHz for $T_2 = 10$ μs. Since this is much smaller than the difference between the energy gaps in the spin Hamiltonian (1), transitions can be spectroscopically resolved.

We now consider a two-qubit logical gate, such as the controlled-phase $C - \varphi$. In the MSQ architecture, this can be realized by considering a molecule consisting of three interacting LQs, where the middle one acts as a switch for the effective coupling between the other two,[78,79] Q_1 and Q_2 (inset of Fig. 3). In the presence of an interaction between the three units, the excitations of the switch are dependent on the states of both Q_1 and Q_2. This allows us to induce a 2π (semi-)resonant excitation of the switch (initialized in $|0_L\rangle$) only for a specific 2-qubit logical state, such as $|1_L 1_L\rangle$. As a result, a phase is added only to

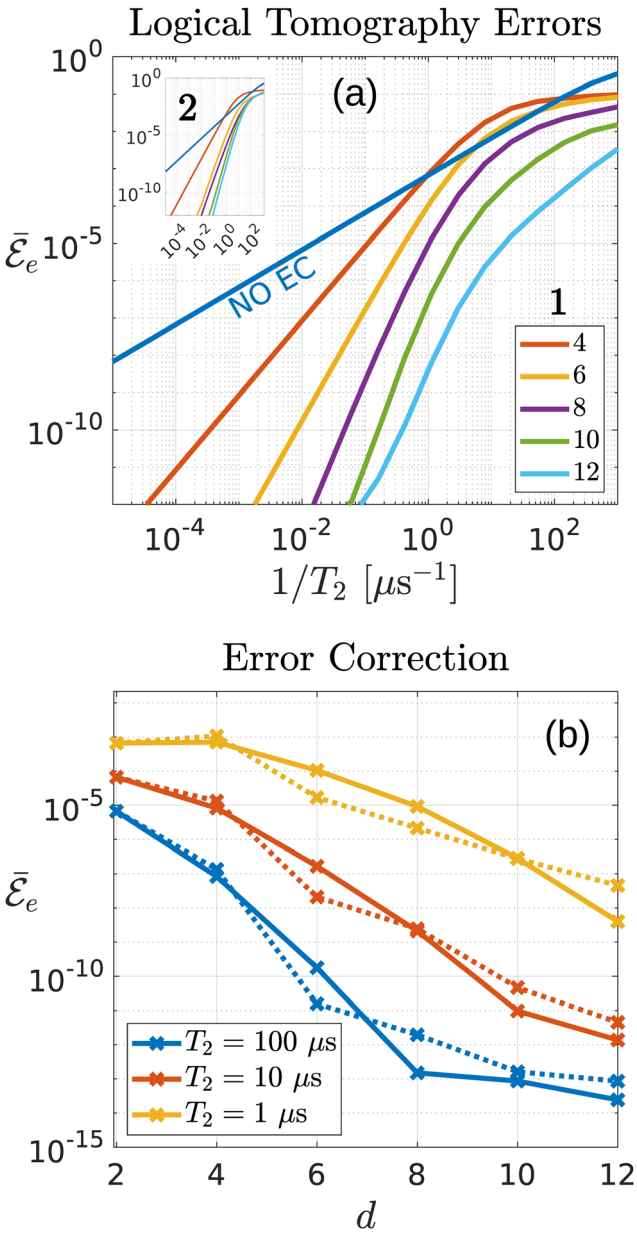

Fig. 2 Simulation of the fault-tolerant implementation of single-qubit logical gates on a MSQ. (a) Logical errors for **1** and **2** (inset) $\bar{\mathscr{E}}_e = 1 - \bar{\mathscr{F}}_e^2$ as a function of $1/T_2$, where $\bar{\mathscr{F}}_e$ is the entanglement fidelity,[72] averaged over different planar rotations $R_L^P(\theta,\varphi)$ for $(\theta,\varphi) = \left(\frac{\pi}{4},\pi\right), \left(\frac{\pi}{2},\pi\right), \left(\frac{\pi}{2},-\frac{\pi}{2}\right), \left(\frac{\pi}{2},-\frac{\pi}{4}\right), \left(\frac{\pi}{2},-\frac{\pi}{8}\right)$. (b) Performance of the code as a function of the number of levels for different values of T_2 for **1** (solid lines) and **2** (dotted lines), indicating a very similar performance. The same driving field amplitude is assumed for manipulating the different LQs and the uncorrected qubit, represented by spin 1/2 with $g = 2$.

ta $|1_L 1_L\rangle$ component of the two-qubit logical state,[65,78–80] *i.e.* a $C - \varphi$ gate is implemented (see also the ESI†).

Since this involves a logical rotation $R_L^P(2\pi,0)$ of the switch, the latter must also be encoded and corrected. The simulation of the two-qubit gate followed by EC on all three units is shown in Fig. 3 for molecules **1** (solid lines) and **2** (dotted lines) with $d = 4, 6$. Here, the performance is slightly better for **2**, where the logical error is suppressed for $T_2 \gtrsim 25$ μs (4-level encoding) and

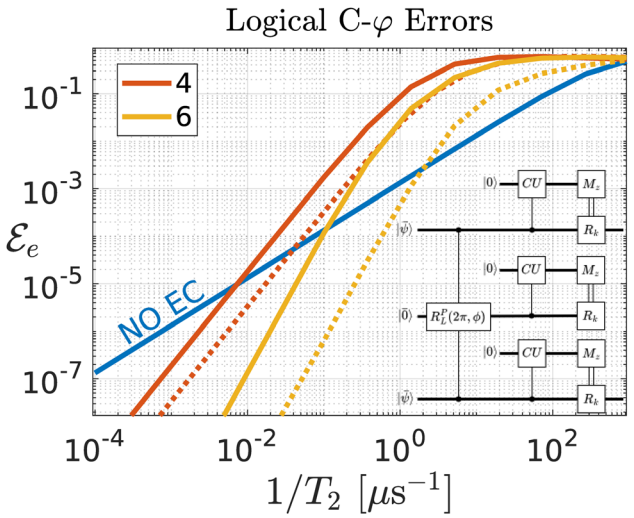

Fig. 3 Numerical simulation of FT implementation of two-qubit logical $C - \varphi$ for **1** (solid lines) and **2** (dotted lines). The logical error is shown as a function of $1/T_2$ at the end of a "logical gate – EC" cycle. Simulations are computationally demanding and hence we limit them to $d = 4, 6$. Inset: Simulated circuit, with external lines corresponding to LQs in a generic logical state $|\bar{\psi}\rangle$, coupled by an error-corrected switch initialized in $|0_L\rangle$ (middle line). Each unit is coupled to a $d/2$-level ancilla for stabilization.

$T_2 \gtrsim 500$ ns (6-level encoding), yielding $p \gtrsim \tau/2T_2 \approx 8\%$. Conversely, the threshold values for **1** are ~100 μs ($S = 3/2$) and ~10 μs ($S = 5/2$). We emphasize that these numbers are within experimental capabilities.[57,73,81]

3 Conclusions

We have shown a fault-tolerant protocol for quantum computation with qudit-embedded stabilizer codes in a molecular spin architecture.[65] Numerical simulations using very different molecular spin qudits highlight the remarkable performance of this approach and the possibility of applying it to a wide range of molecules. This embedded protocol prevents the blowing up of the number of physical units typical of multi-qubit codes while yielding a large error suppression with a small number of qudit levels. This makes the novel concept we introduce very appealing for actual implementation and demonstrates the potential of molecular spin materials. In particular, we have shown that simple molecules consisting of a single magnetic ion (or, in general, a giant spin S) can represent a new generation of logical qubits. The only requirement of the system is a significant anisotropy, while coherence times need not be particularly high. This places the proposed platform well within the capabilities of synthetic chemistry.[46,47] Moreover, nuclear spins (common to most molecular systems) provide another interesting platform for encoding error-protected logical qubits. Although the implementation of the whole FTQC scheme with large-spin nuclear qudits is challenging, this setup can be used for proof-of-principle experiments on a limited number of levels, such as a nuclear spin 3/2 coupled to an electronic spin 1/2. Indeed, the electronic

spin could be exploited as an ancilla both for fastening nuclear spin manipulation[82–84] and for nuclear spin readout.[19,66]

Finally, the conditions we have pinpointed, *i.e.* a well-defined hierarchy of errors and proper connectivity between the system eigenstates, trace a clear route to extend the proposed strategies also to other qudit platforms.

Author contributions

Conceptualization: A. C., and S. C.; methodology: M. M., and A. C.; software: M. M.; formal analysis: M. M. and A. C.; investigation: M. M., A. C., L. L., and S. C.; writing (original draft): A. C. and M. M.; writing (review and editing): L. L. and S. C.; supervision: S. C.; project administration: S. C.; and funding acquisition: S. C.

Data availability

Data for this article, including all the data for the plots in the article, are available on Zenodo at **https://zenodo.org/doi/10.5281/zenodo.11956801**.

Conflicts of interest

There are no conflicts to declare.

Acknowledgements

We warmly thank P. Santini for useful and stimulating discussions. This work received funding from the European Union – NextGenerationEU, PNRR MUR project PE0000023-NQSTI, from Novo Nordisk Foundation under grant NNF21OC0070832 in the call ''Exploratory Interdisciplinary Synergy Programme 2021'', from the European Unions Horizon 2020 program under Grant Agreement No. 862893 (FET-OPEN project FATMOLS) and from Fondazione Cariparma. M. M. acknowledges funding from the European Union – NextGenerationEU under the National Recovery and Resilience Plan (NRRP), Mission 4 Component 1 Investment 3.4 and 4.1. Decree by the Italian Ministry no. 351/2022 CUP D92B22000530005.

References

§ This is consistent with the re-scaling of the zero-field splitting anisotropy, theoretically predicted and experimentally observed in single-molecule magnets.[45]

¶ In general, one should include a sum over different components $C^{\alpha\alpha'}_{kk'}$ with $\alpha\alpha' = x, y, z$. However, in both systems **1** and **2**, only $\alpha = \alpha' = z$ terms contribute. This depends in the former case on the form of the zero-field splitting term which only connects $\Delta M = \pm 2$ eigenstates of S_z, and in the latter on the axial symmetry of the spin Hamiltonian (see the ESI†).

‖ The relative phase between $|\ell,k\rangle|0\rangle$ and $|\ell,k\rangle|k\rangle$ is necessary to ensure that the corresponding generator has zero diagonal. Since the ancilla is initialized in $|0\rangle$, this relative phase is irrelevant.

** This is due to the specific form of the error words $\{|\ell,k\rangle\}$, in which the two $\ell = 0, 1$ subspaces are disjoint for all k.

†† This allows us to compare the performance of a spin 1/2 qubit (without EC) and of the LQ even though the duration of the elementary transitions on them is different (and hence the related error probability). Indeed, the elementary error probability for a two-level system is $p = (1 - \exp[-\tau/T_2])/2$.[58] Since the duration τ of the transition is much smaller for spin 1/2, it would result in a much smaller p compared to the LQ, thus making the comparison unfair.

‡‡ $\mathscr{F}_e$ is the average fidelity on the initial states $|0_L\rangle, |1_L\rangle, \frac{1}{\sqrt{2}}(|0_L\rangle + |1_L\rangle), \frac{1}{\sqrt{2}}(|0_L\rangle - |1_L\rangle), \frac{1}{\sqrt{2}}(|0_L\rangle + i|1_L\rangle), \frac{1}{\sqrt{2}}(|0_L\rangle - i|1_L\rangle)$.

§§ We made the conservative assumption of setting the same duration of the pulses independent of S and corresponding to the smallest matrix elements (those of the largest spin). By fixing the driving field, the performance for the lowest and most common spins $S \leq 7/2$ would further improve.

1 R. Chao and B. W. Reichardt, *npj Quantum Inf.*, 2018, **4**, 42.
2 D. Gottesman, *An Introduction to Quantum Error Correction*, 2000.
3 S. J. Devitt, W. J. Munro and K. Nemoto, *Rep. Prog. Phys.*, 2013, **76**, 076001.
4 D. Nigg, M. Müller, E. A. Martinez, P. Schindler, M. Hennrich, T. Monz, M. A. Martin-Delgado and R. Blatt, *Science*, 2014, **345**, 302–305.
5 B. M. Terhal, *Rev. Mod. Phys.*, 2015, **87**, 307–346.
6 E. Campbell, B. Terhal and C. Vuillot, *Nature*, 2017, **549**, 172–179.
7 P. Aliferis, D. Gottesman and J. Preskill, *Quantum Inf. Comput.*, 2006, **6**, 97–165.
8 E. Knill, *Nature*, 2005, **434**, 39–44.
9 A. W. Cross, D. P. Divincenzo and B. M. Terhal, *Quantum Inf. Comput.*, 2009, **9**, 541–572.
10 D. S. Wang, A. G. Fowler and L. C. L. Hollenberg, *Phys. Rev. A: At., Mol., Opt. Phys.*, 2011, **83**, 020302.
11 A. G. Fowler, A. M. Stephens and P. Groszkowski, *Phys. Rev. A: At., Mol., Opt. Phys.*, 2009, **80**, 052312.
12 A. G. Fowler, M. Mariantoni, J. M. Martinis and A. N. Cleland, *Phys. Rev. A: At., Mol., Opt. Phys.*, 2012, **86**, 032324.
13 A. M. Stephens, *Phys. Rev. A: At., Mol., Opt. Phys.*, 2014, **89**, 022321.
14 C. Chamberland, T. Jochym-O'Connor and R. Laflamme, *Phys. Rev. Lett.*, 2016, **117**, 010501.
15 J. Marks, T. Jochym-OConnor and V. Gheorghiu, *New J. Phys.*, 2017, **19**, 113022.
16 E. T. Campbell, *Phys. Rev. Lett.*, 2014, **113**, 230501.
17 M. Suchara, J. Kubiatowicz, A. Faruque, F. T. Chong, C.-Y. Lai and G. Paz, 2013 IEEE 31st International Conference on Computer Design (ICCD), 2013, pp. 419–426.
18 A. Paetznick, C. Knapp, N. Delfosse, B. Bauer, J. Haah, M. B. Hastings and M. P. da Silva, *PRX Quantum*, 2023, **4**, 010310.
19 A. Chiesa, E. Macaluso, F. Petiziol, S. Wimberger, P. Santini and S. Carretta, *J. Phys. Chem. Lett.*, 2020, **11**, 8610–8615.
20 F. Petiziol, A. Chiesa, S. Wimberger, P. Santini and S. Carretta, *npj Quantum Inf.*, 2021, **7**, 133.
21 S. Carretta, D. Zueco, A. Chiesa, A. Gómez-León and F. Luis, *Appl. Phys. Lett.*, 2021, **118**, 240501.
22 M. Atzori and R. Sessoli, *J. Am. Chem. Soc.*, 2019, **141**, 11339.
23 A. Chiesa, F. Petiziol, M. Chizzini, P. Santini and S. Carretta, *J. Phys. Chem. Lett.*, 2022, **13**, 6468–6474.
24 A. L. Grimsmo, J. Combes and B. Q. Baragiola, *Phys. Rev. X*, 2020, **10**, 011058.

25 S. Pirandola, S. Mancini, S. L. Braunstein and D. Vitali, *Phys. Rev. A: At., Mol., Opt. Phys.*, 2008, **77**, 032309.
26 C. Cafaro, F. Maiolini and S. Mancini, *Phys. Rev. A: At., Mol., Opt. Phys.*, 2012, **86**, 022308.
27 M. H. Michael, M. Silveri, R. Brierley, V. V. Albert, J. Salmilehto, L. Jiang and S. M. Girvin, *Phys. Rev. X*, 2016, **6**, 031006.
28 W. Cai, Y. Ma, W. Wang, C.-L. Zou and L. Sun, *Fundam. Res.*, 2021, **1**, 50–67.
29 M. Chizzini, L. Crippa, L. Zaccardi, E. Macaluso, S. Carretta, A. Chiesa and P. Santini, *Phys. Chem. Chem. Phys.*, 2022, **24**, 20030.
30 S. Lim, J. Liu and A. Ardavan, *Fault-tolerant qubit encoding using a spin-7/2 qudit*, 2023.
31 S. Omanakuttan and J. A. Gross, Multispin Clifford codes for angular momentum errors in spin systems, 2023.
32 P. Reinhold, S. Rosenblum, W.-L. Ma, L. Frunzio, L. Jiang and R. J. Schoelkopf, *Nat. Phys.*, 2020, **16**, 822–826.
33 S. Puri, L. St-Jean, J. A. Gross, A. Grimm, N. E. Frattini, P. S. Iyer, A. Krishna, S. Touzard, L. Jiang, A. Blais, S. T. Flammia and S. M. Girvin, *Sci. Adv.*, 2020, **6**, eaay5901.
34 S. Rosenblum, P. Reinhold, M. Mirrahimi, L. Jiang, L. Frunzio and R. J. Schoelkopf, *Science*, 2018, **361**, 266–270.
35 L. Hu, Y. Ma, W. Cai, X. Mu, Y. Xua, W. Wang, Y. Wu, H. Wang, Y. P. Song, C.-L. Zou, S. M. Girvin, L.-M. Duan and L. Sun, *Nat. Phys.*, 2019, **15**, 503–508.
36 Z. Ni, S. Li, X. Deng, Y. Cai, L. Zhang, W. Wang, Z.-B. Yang, H. Yu, F. Yan, S. Liu, C.-L. Zou, L. Sun, S.-B. Zheng, Y. Xu and D. Yu, *Nature*, 2023, **616**, 56–60.
37 Y. Ma, Y. Xu, X. Mu, W. Cai, L. Hu, W. Wang, X. Pan, H. Wang, Y. P. Song, C.-L. Zou and L. Sun, *Nat. Phys.*, 2020, **16**, 827–831.
38 S. T. Liddle and J. van Slageren, *Chem. Soc. Rev.*, 2015, **44**, 6655.
39 J.-L. Liu, Y.-C. Chen and M.-L. Tong, *Chem. Soc. Rev.*, 2017, **47**, 2431.
40 C. A. P. Goodwin, F. Ortu, D. Reta, N. F. Chilton and D. P. Mills, *Nature*, 2017, **548**, 439.
41 F.-S. Guo, B. M. Day, Y.-C. Chen, M.-L. Tong, A. Mansikkamäki and R. A. Layfield, *Science*, 2018, **362**, 1400.
42 A. Chiesa, F. Cugini, R. Hussain, E. Macaluso, G. Allodi, E. Garlatti, M. Giansiracusa, C. A. P. Goodwin, F. Ortu, D. Reta, J. M. Skelton, T. Guidi, P. Santini, M. Solzi, R. De Renzi, D. P. Mills, N. F. Chilton and S. Carretta, *Phys. Rev. B*, 2020, **101**, 174402.
43 M. Murugesu, S. Takahashi, A. Wilson, K. A. Abboud, W. Wernsdorfer, S. Hill and G. Christou, *Inorg. Chem.*, 2008, **47**, 9459–9470.
44 L. Qin, H.-L. Zhang, Y.-Q. Zhai, H. Nojiri, C. Schröder and Y.-Z. Zheng, *iScience*, 2021, **24**, 102350.
45 O. Waldmann, *Inorg. Chem.*, 2007, **46**, 10035–10037.
46 M. Fataftah, J. M. Zadrozny, S. C. Coste, M. J. Graham, D. M. Rogers and D. E. Freedman, *J. Am. Chem. Soc.*, 2016, **138**, 1344.
47 M. D. Jenkins, Y. Duan, B. Diosdado, J. J. García-Ripoll, A. Gaita-Ariño, C. Giménez-Saiz, P. J. Alonso, E. Coronado and F. Luis, *Phys. Rev. B*, 2017, **95**, 064423.
48 M. Chizzini, L. Crippa, A. Chiesa, F. Tacchino, F. Petiziol, I. Tavernelli, P. Santini and S. Carretta, *Phys. Rev. Res.*, 2022, **4**, 043135.
49 E. Knill and R. Laflamme, *Phys. Rev. A: At., Mol., Opt. Phys.*, 1997, **55**, 900–911.
50 C. D. Bruzewicz, J. Chiaverini, R. McConnell and J. M. Sage, *Appl. Phys. Lett.*, 2019, **6**, 021314.
51 M. Ringbauer, M. Meth, L. Postler, R. Stricker, R. Blatt, P. Schindler and T. Monz, *Nat. Phys.*, 2022, **18**, 1053–1057.
52 S. Kuhr, W. Alt, D. Schrader, I. Dotsenko, Y. Miroshnychenko, A. Rauschenbeutel and D. Meschede, *Phys. Rev. A: At., Mol., Opt. Phys.*, 2005, **72**, 023406.
53 A. Morello, J. J. Pla, P. Bertet and D. N. Jamieson, *Adv. Quantum Technol.*, 2020, **3**, 2000005.
54 A. Chatterjee, P. Stevenson, S. De Franceschi, A. Morello, N. P. de Leon and F. Kuemmeth, *Nat. Rev. Phys.*, 2021, **3**, 157–177.
55 K. Bader, M. Winkler and J. van Slageren, *Chem. Commun.*, 2016, **52**, 3623–3626.
56 Y.-S. Ding, Y.-F. Deng and Y.-Z. Zheng, *Magnetochemistry*, 2016, **2**, 40.
57 K. Bader, D. Dengler, S. Lenz, B. Endeward, S.-D. Jiang, P. Neugebauer and J. van Slageren, *Nat. Commun.*, 2014, **5**, 5304.
58 M. A. Nielsen and I. L. Chuang, *Quantum Computation and Quantum Information*, Cambridge University Press, 2000.
59 M. N. Leuenberger and D. Loss, *Phys. Rev. B: Condens. Matter Mater. Phys.*, 2003, **68**, 165317.
60 A. G. Fowler, A. C. Whiteside and L. C. L. Hollenberg, *Phys. Rev. Lett.*, 2012, **108**, 180501.
61 S. Bravyi, M. Suchara and A. Vargo, *Phys. Rev. A: At., Mol., Opt. Phys.*, 2014, **90**, 032326.
62 P. Das, C. A. Pattison, S. Manne, D. M. Carmean, K. M. Svore, M. Qureshi and N. Delfosse, 2022 IEEE International Symposium on High-Performance Computer Architecture (HPCA), 2022, pp. 259–273.
63 R. Sweke, M. S. Kesselring, E. P. L. van Nieuwenburg and J. Eisert, *Mach. Learn.: Sci. Technol.*, 2020, **2**, 025005.
64 I. Gimeno, W. Kersten, M. Pallarés, P. Hermosilla, M. Martínez-Pérez, M. Jenkins, A. Angerer, C. Sánchez-Azqueta, D. Zueco, J. Majer, A. Lostao and F. Luis, *ACS Nano*, 2020, **14**, 8707.
65 A. Chiesa, S. Roca, S. Chicco, M. de Ory, A. Gómez-León, A. Gomez, D. Zueco, F. Luis and S. Carretta, *Phys. Rev. Appl.*, 2023, **19**, 064060.
66 S. J. Lockyer, A. Chiesa, G. A. Timco, E. J. L. McInnes, T. S. Bennett, I. J. Vitorica-Yrezebal, S. Carretta and R. E. P. Winpenny, *Chem. Sci.*, 2021, **12**, 9104.
67 S. J. Lockyer, A. Chiesa, A. Brookfield, G. A. Timco, G. F. S. Whitehead, E. J. L. McInnes, S. Carretta and R. E. P. Winpenny, *J. Am. Chem. Soc.*, 2022, **144**, 16086–16092.

68 C. J. Rogers, D. Asthana, A. Brookfield, A. Chiesa, G. A. Timco, D. Collison, L. S. Natrajan, S. Carretta, R. E. P. Winpenny and A. M. Bowen, *Angew. Chem., Int. Ed.*, 2022, e202207947.
69 S. Nakazawa, S. Nishida, T. Ise, T. Yoshino, N. Mori, R. D. Rahimi, K. Sato, Y. Morita, K. Toyota, D. Shiomi, M. Kitagawa, H. Hara, P. Carl, P. Höfer and T. Takui, *Angew. Chem., Int. Ed.*, 2012, **51**, 9860–9864.
70 B. K. Rugg, M. D. Krzyaniak, B. T. Phelan, M. A. Ratner, R. M. Young and M. R. Wasielewski, *Nat. Chem.*, 2019, **11**, 981–986.
71 J. H. Olshansky, S. M. Harvey, M. L. Pennel, M. D. Krzyaniak, R. D. Schaller and M. R. Wasielewski, *J. Am. Chem. Soc.*, 2020, **142**, 13590–13597.
72 E. Knill, R. Laflamme, R. Martinez and C. Negrevergne, *Phys. Rev. Lett.*, 2001, **86**, 5811–5814.
73 M. Atzori, E. Morra, L. Tesi, A. Albino, M. Chiesa, L. Sorace and R. Sessoli, *J. Am. Chem. Soc.*, 2016, **138**, 11234–11244.
74 M. Atzori, L. Tesi, E. Morra, M. Chiesa, L. Sorace and R. Sessoli, *J. Am. Chem. Soc.*, 2016, **138**, 2154–2157.
75 M. Atzori, E. Garlatti, G. Allodi, S. Chicco, A. Chiesa, A. Albino, R. D. Renzi, E. Salvadori, M. Chiesa, S. Carretta and L. Sorace, *Inorg. Chem.*, 2021, **60**, 11273–11286.
76 A. Kandala, A. Mezzacapo, K. Temme, M. Takita, M. Brink, J. M. Chow and J. M. Gambetta, *Nature*, 2017, **549**, 242–246.
77 A. Castro, A. García Carrizo, S. Roca, D. Zueco and F. Luis, *Phys. Rev. Appl.*, 2022, **17**, 064028.
78 J. Ferrando-Soria, E. Moreno-Pineda, A. Chiesa, A. Fernandez, S. A. Magee, S. Carretta, P. Santini, I. Vitorica-Yrezabal, F. Tuna, E. J. L. McInness and R. E. P. Winpenny, *Nat. Commun.*, 2016, **7**, 11377.
79 A. Chiesa, F. Petiziol, E. Macaluso, S. Wimberger, P. Santini and S. Carretta, *AIP Adv.*, 2021, **11**, 025134.
80 A. Chiesa, G. F. S. Whitehead, S. Carretta, L. Carthy, G. A. Timco, S. J. Teat, G. Amoretti, E. Pavarini, R. E. P. Winpenny and P. Santini, *Sci. Rep.*, 2014, **4**, 7423.
81 J. M. Zadrozny, J. Niklas, O. G. Poluektov and D. E. Freedman, *ACS Cent. Sci.*, 2015, **1**, 488–492.
82 R. Hussain, G. Allodi, A. Chiesa, E. Garlatti, D. Mitcov, A. Konstantatos, K. Pedersen, R. D. Renzi, S. Piligkos and S. Carretta, *J. Am. Chem. Soc.*, 2018, **140**, 9814–9818.
83 S. Chicco, A. Chiesa, G. Allodi, E. Garlatti, M. Atzori, L. Sorace, R. De Renzi, R. Sessoli and S. Carretta, *Chem. Sci.*, 2021, **12**, 12046.
84 I. Gimeno, A. Urtizberea, J. Román-Roche, D. Zueco, A. Camón, P. J. Alonso, O. Roubeau and F. Luis, *Chem. Sci.*, 2021, **12**, 5621–5630.